Analytica Chimica Acta 1148 (2021) 338201

Contents lists available at ScienceDirect

Analytica Chimica Acta

journal homepage: www.elsevier.com/locate/aca

Integration of fluorescent polydopamine nanoparticles on protamine for simple and sensitive trypsin assay

Fenglan Li [a, 1], Yiping Chen [b, 1], Renxi Lin [d], Chenfang Miao [a], Jiahui Ye [a], Qianqian Cai [a], Zhengjun Huang [a], Yanjie Zheng [a], Xinhua Lin [a], Zongfu Zheng [c, **], Shaohuang Weng [a, *]

[a] Department of Pharmaceutical Analysis, School of Pharmacy, Higher Educational Key Laboratory for Nano Biomedical Technology of Fujian Province, Fujian Medical University, Fuzhou, 350122, China
[b] Department of Interventional Radiology, The First Affiliated Hospital of Fujian Medical University, Fuzhou, 350005, China
[c] The 900th Hospital of PLA, Fuzhou, 350002, China
[d] School of Basic Medical Sciences, Fujian Medical University, Fuzhou, 350122, China

HIGHLIGHTS

- Stable fluorescent negatively charged polydopamine nanoparticles (PDNPs) are obtained through a controllable method.
- PDNPs directly integrate with protamine (Pro) to form an aggregation-caused quenching system (PDNPs-Pro).
- The formation of the PDNPs-Pro is due to surface charge, hydrogen bond, and appropriate size of PDNPs.
- Fluorescence recovery of PDNPs in PDNPs-Pro is used to monitor the trypsin via the hydrolysis of Pro by trypsin.
- This strategy opens up a new sight about the functional polymers for biomedical applications using simple chemical operation.

GRAPHICAL ABSTRACT

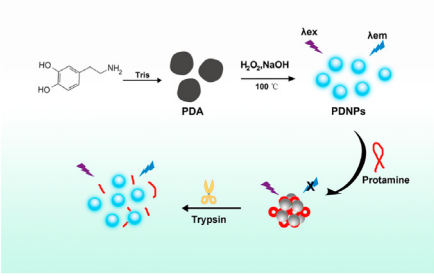

ARTICLE INFO

Article history:
Received 25 November 2020
Received in revised form
3 January 2021
Accepted 5 January 2021
Available online 7 January 2021

Keywords:
Negatively charged polydopamine nanoparticles

ABSTRACT

As an important protease, trypsin (TRY) has been identified as a key indicator of various diseases. A simple and sensitive strategy for TRY detection by using an environment-friendly biosafe probe is significant. Herein, we introduced negatively charged fluorescent polydopamine nanoparticles (PDNPs) with 4.8 nm diameter obtained through a controllable method as an effective probe for TRY. PDNPs exhibited excellent fluorescence property but integrated with protamine (Pro) to form an aggregation-caused quenching system via a static quenching mechanism. The quenching mechanism of Pro to PDNPs revealed the significant effect of the surface charge, functional groups, and appropriate size of PDNPs on quenching process. Given the specific hydrolysis of Pro by TRY, PDNPs were released from the quenching integration of PDNPs and Pro (PDNPs-Pro) and recovered their fluorescence. Thus, a fluorescence sensor for TRY with a linear range of 0.01 and 0.1 μg/mL and a detection limit of 6.7 ng/mL was

* Corresponding author.
** Corresponding author.
E-mail addresses: fuhos_476@126.com (Z. Zheng), shweng@fjmu.edu.cn (S. Weng).
[1] Both of the authors contributed equally.

https://doi.org/10.1016/j.aca.2021.338201

Protamine
Integration
Sensitive fluorescence strategy
Trypsin

developed without the disturbing from other proteases. Compared with other TRY assays, the biosensor based on PDNPs-Pro has the advantages of simple operation, environmental friendliness, and high sensitivity. This specific controlled-synthesis PDNPs would open up a new window for the extended application of fluorescent nanomaterials in biomedicine based on fluorescence changes induced by biological interaction.

1. Introduction

Protease is a proteolytic hydrolase, which involves various biological and physiological processes, including digestion, coagulation, cell apoptosis, and a series of other cellular activities [1,2]. Trypsin (TRY) is one of the most important digestive proteases and plays an important role in regulating pancreatic exocrine function [3]. In general, TRY is overexpressed in acute pancreatitis, cystic fibrosis, and pancreatic cancer [4,5]. Several strategies, including enzyme-linked immunosorbent assay [6], colorimetry [1,5], chemiluminescence [7], electrochemical immunoassay [8], photoelectrochemistry [9], and fluorescence method [10] have been fabricated for TRY monitoring. Among such methods, the fluorescent assay is promising because of its simplicity, high sensitivity, rapid implementation, and real-time detection [11,12]. To date, the fluorescent assays for TRY based on gold nanoparticles [13], quantum dots (QDs) [14], conjugated polymer dots [15], and organic dyes [16], have been reported. Most of these methods were designed in accordance with TRY modulation toward fluorescent probe and protein interaction based on fluorescence resonance energy transfer [13], or inner-filter effect [14], or aggregation-caused quenching [15,16]. Thus, the fabrication of an appropriate interaction system between a specific probe and a protein substrate is the key section. Compared with the primary tedious chemical synthetic process between response active sites and probes [9,15,17,18], the focus of fluorescence assays shifts to the construction of the direct interaction of substrate and probes through single mixing step with possible sustainable application [10,13]. For fluorescent probes, the controllable surface properties with the proper physical size is essential for the performance of the fabricated fluorescent strategy [19,20]; as such, target bioanalytes (especially large biomolecules) may directly approach certain sites of the probes [21,22] and may induce the quenching or enhancement of the fluorescence property of nanoparticles [23] through photo-induced electron transfer [24,25] or aggregation-caused quenching [26,27]. Thus, several factors, such as surface charges, physical size, mode of action, and assembly behavior of quantum dots, should be considered in the fabrication of the system of nanoparticles and organisms [13,28,29].

Recently, fluorescent polymer dots have emerged as a kind of promising material due to their size controllability, remarkable stability, biocompatibility, and easy to modify in the biological environment [30–33]. Dopamine is one of the biogenic neurotransmitters that play an important role in biological activity. Moreover, dopamine can be changed into polydopamine (PDA) with variable morphologies through covalent bonding, hydrogen bonding, and $\pi-\pi$ interaction [34,35]. PDA has emerged as a new type of biopolymer material with applications in biomedicine, surface coating, energy materials, and sewage treatment because of its remarkable functional properties and excellent biocompatibility [36,37]. Compared with the common non-fluorescence polydopamine with large size applied as probe carrier for bioanalysis [38–40], dopamine can also be converted to fluorescent nanostructured polydopamine (F-PDA) through certain controlled synthetic approaches for bioanalytical applications through the interaction between F-PDA and specific assistants [41–46]. The interaction between F-PDA and metal ions through coordination [44] or the absorption system of F-PDA nanoparticles on metal oxide nanosheets [45] is an effective tool for detecting target analyte. However, studies that reported the analytical strategy for TRY based on the direct interaction between F-PDA and biomacromolecules, such as proteins, are rare. The reason for the above blank may be due to the hard control of the interaction between proteins and F-PDA with the appropriate surface property, functional groups, and size.

To sum up the above analysis, we hypothesized that the integration of F-PDA and biomolecules was an attractive procedure that F-PDA served as fluorescence source and building blocks for assembly. In general, different surface properties PDA nanoparticles with variable diameters will be obtained with modulated surface functional groups, like the outward −OH induced negative charged PDA. Thus, inspired with the possible surface interaction of polydopamine [47] and our recent works about the control of the surface property of carbon dots to achieve carbon dots aggregation and DNA interaction [48–50], we designed an F-PDA with appropriate surface property and suitable physical size to interact and assemble with protamine (Pro) accompanied by changeable fluorescence behavior. As shown in Scheme 1, a controlled diameter negatively charged fluorescent polydopamine nanoparticles (PDNPs) were prepared and applied to interact with positive Pro to fabricate an aggregation-induced quenching system of PDNPs and Pro (PDNPs-Pro). Given the selective enzymolysis of TRY toward arginine, arginine-rich protamine will be destroyed to promote PDNPs release from PDNPs-Pro, thereby motivating the recovery of the fluorescence for TRY quantification. This method illustrates the characteristics of simplicity, green preparation, sensitivity and selectivity for the TRY monitor. Furthermore, this work suggests that the combination of PDNPs with proteins and other potential biomolecules may lead to a class of controllable property of

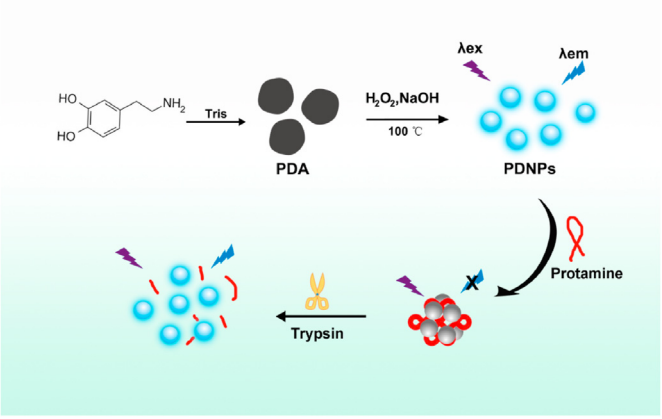

Scheme 1. Detection of TRY based on the integration of PDNPs and Pro.

biomaterials with a bright application prospect in diagnosis and clinical treatment via a facile strategy.

2. Experimental section

2.1. Materials and apparatus

Dopamine hydrochloride, trypsin (TRY), protamine (Pro), Bovine serum albumin (BSA), acid phosphatase (ACP), tyrosinase (Tyr), and hyaluronidase were purchased from Sigma-Aldrich. Pepsin (Pep) and Chymotrypsin (Chy) were from Beijing Solarbio Science & Technology Co., Ltd. Papain (Pap) was provided by Sangon Biotech (Shanghai) Co., Ltd. Cell counting kit-8 (CCK8) kit was obtained from Beyotime Biotechnology. Metal salts (NaCl, KCl, $CaCl_2$, and so on), Tris(hydroxymethyl)aminomethane (Tris), urea, and glucose were obtained from Sinopharm Chemical Reagent Co., Ltd. Phosphate Buffer (PB) prepared from $NaH_2PO_4 \cdot 2H_2O$ and $Na_2HPO_4 \cdot 12H_2O$ was used as reacting buffer in this work unless otherwise specified. Without any special instructions, all of the materials were used as received. Milli-Q purified water (18.2 MΩ cm) was used for all experiments.

All fluorescence spectra were recorded through Cary Eclipse Fluorescence Spectrophotometer. UV−vis absorption spectra were measured on a UV-2250 spectrophotometer. Transmission electron microscopy (TEM) images were conducted on a FEI Talos F200. Fourier transform infrared (FTIR) spectra were recorded with a NICOLET iS50 Infrared Spectroscopy. Zeta potential measurements were performed with an Anton Paar Litesizer 500 at 25 °C.

2.2. Synthesis of PDNPs

Dopamine hydrochloride (0.05 g) and Tris (0.0606 g) were completely dissolved in 40 mL ultrapure water to prepare PDA nanoparticles under gentle stirring for 20 h. The obtained PDA nanoparticles were cut down in a solution containing H_2O_2 (20%, 15 mL) and NaOH (2.5 M, 10 mL) with reflux at 100 °C for 30 min. In the cutting process, the color of the solution changed from black to yellow. Then, the cooled above solution was purified through dialysis (MW: 3500 Da) over water and ethanol to remove the hydroxyl radical and unreacted agents to obtain PDNPs. Finally, the purified PDNPs were lyophilized. A certain weight of the solid state PDNPs was accurately tested using electronic balance for the preparation of PDNPs dispersion for the further use.

2.3. Cytotoxicity assay

The possible cytotoxicity of PDNPs was measured via CCK8. A549 cells were seeded in 96-well plates at a density of 4×10^3 cells per well. The cells were incubated for 24 h at 37 °C and 5% CO_2 incubator for attachment. PDNPs with different concentrations (500, 300, 200, 100, and 50 μg/mL) were added and incubated for another 24 h. Next, 10 μL of CCK8 was added to the wells and incubated for another 2 h. The optical density (OD) at 450 nm was measured using a microplate reader.

2.4. Assay for TRY activity

A 40 μL of Pro (40 μg/mL) and 100 μL of PDNPs (0.15 μg/mL) were added to 50 μL of PB (pH 8.0, 10 mM) and incubated for 2 min at 37 °C. Then, 10 μL of TRY at different concentrations were mixed with the above PDNPs and Pro complex (PDNPs-Pro). After the samples were reacted in the dark for 45 min at 37 °C, their fluorescence spectra were recorded. The excitation and emission slits were set at 5 and 10 nm, respectively. Selectivity experiments were carried out under the same procedure. All experiments were performed in triplicates. Error bars showed the standard deviation (SD) of the parallel testing. In the testing process, fluorescence enhancement efficiency ($(F-F_0)/F_0$) was applied to quantify the TRY activity. F and F_0 were the fluorescence intensity of PDNPs-Pro in the presence and absence of TRY, respectively.

2.5. Selectivity for TRY activity

Considering the presence of some interference and other digestive enzymes in clinical samples, the selectivity of this method was evaluated through two testing routines. The common interferences (10 μg/mL of KCl, NaCl, $CaCl_2$, glucose, urea, BSA, and Pap) and other enzymes (1.2 U/mL of ACP、Tyr, hyaluronidase, Chy, and Pep) were respectively added into PDNPs-Pro like the procedure of TRY assay with the corresponding fluorescence measurement. Furthermore, according to the same monitoring procedure, the mixture of the respective interference and 0.1 μg/mL TRY were correspondingly added to PDNPs-Pro to investigate the fluorescence response compared with that of pure TRY addition.

2.6. Serum sample assay

Fresh human serum samples with signed informed consent were obtained from volunteers at the 900th Hospital of PLA with the permission of the Ethics Committee. Serum samples were centrifuged at 10000 rpm for 10 min at 4 °C. Then, the supernatants were diluted 10 times with PB (pH 8.0) before use. The procedure for the serum samples assay was according to that used to obtain the calibration curve.

3. Results and discussion

3.1. Structure, optical properties, and biocompatibility of PDNPs

Firstly, the morphology of PDNPs was investigated. As shown in Fig. 1A, PDNPs exhibited uniform sphere morphology, and the average diameter was approximately 4.8 nm. However, the prepared PDA nanoparticles before slash were about 400 nm (Fig. 1B). The apparent difference in the size of PDNPs and the PDA nanoparticles demonstrated that the hydroxyl radical-mediated degradation of PDA nanoparticles to small particle PDNPs because H_2O_2 dissociated to hydroxyl radicals at high NaOH concentrations [51]. FTIR was further carried out to analyze the surface chemical composition of PDNPs. As illustrated in Fig. 1C, the FTIR spectra of the PDA nanoparticles and PDNPs exhibited similar major absorption bands, such as the bands ascribed to C═C and O−H located at 1617 and 3441 cm^{-1}, respectively. The absorption peak at 1635 cm^{-1} was attributed to the stretching vibration of aromatic C═C bonds of indole in PDNPs [52]. The characteristic broad absorption located at 3431 cm^{-1} represented the stretching vibration of O−H and N−H in phenolic hydroxyl. An additional peak centered at 1397 cm^{-1} was attributed to the O−H deformation vibration [51]. The widespread presence of −OH of PDNPs will induce PDNPs negatively charged [53], which was revealed by the tested zeta potential of −3.9 mV.

The optical properties of PDNPs were further investigated. Compared with the DA spectrum with an obvious absorption peak at 280 nm, the spectrum of the PDA nanoparticles showed a decreased absorption at 280 nm ascribed to DA monomer, whereas the broad absorption of 200 nm−500 nm ascribed to the 5,6-dihydroxyindole unit formation started to appear (blue line in Fig. 1D) [54]. The changed absorption spectrum indicated the transfer of the DA monomer to polydopamine during oxidation. PDNPs only showed a wide absorption band from 200 nm to 450 nm with the complete disappearance of the unoxidized

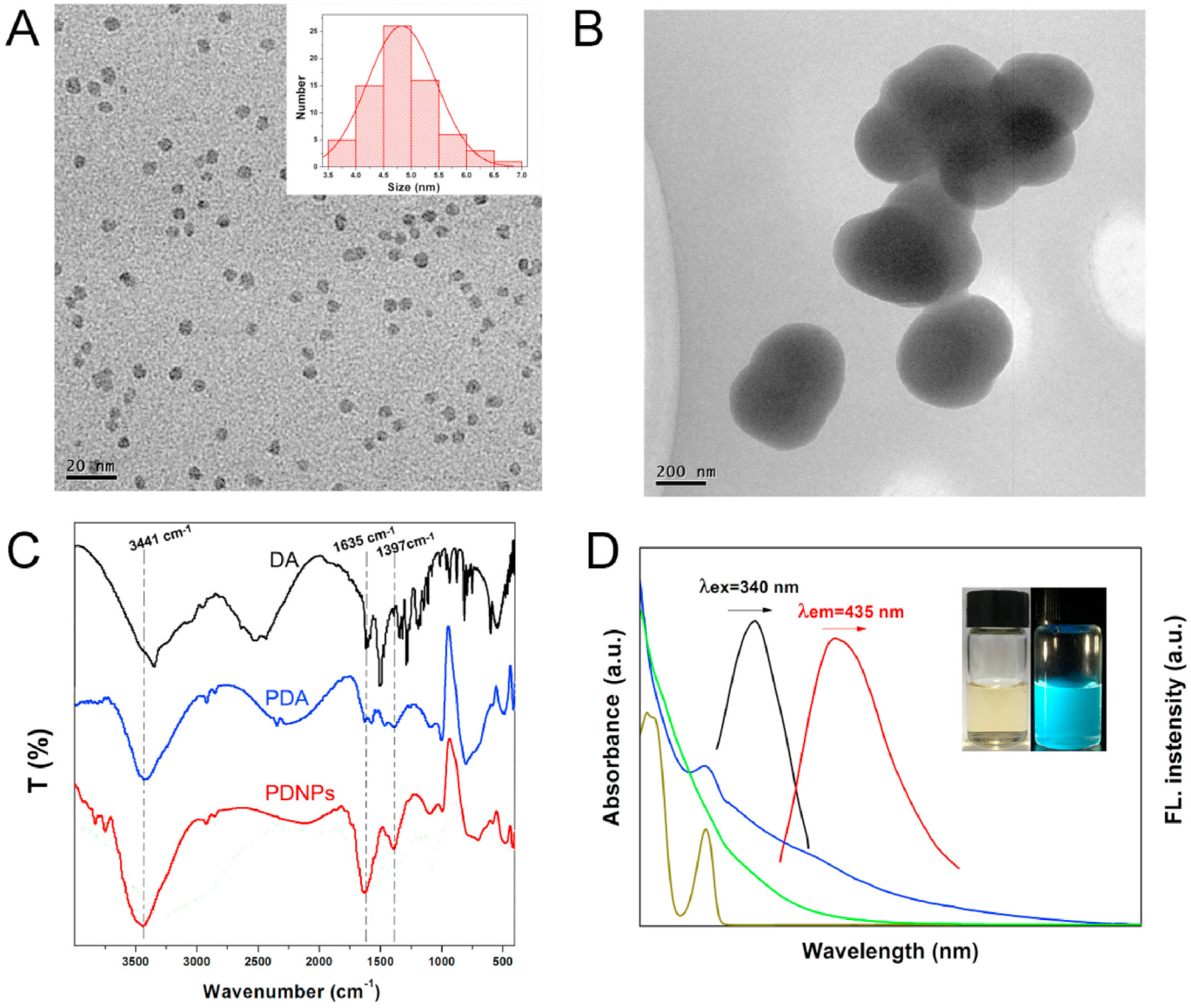

Fig. 1. TEM images of (A) PDNPs and (B) PDA nanoparticles. (C) FTIR spectra of DA, PDA nanoparticles, and PDNPs. (D) UV–vis absorption spectra (left arrow) of DA (brown line), PDA nanoparticles (blue line), PDNPs (green line), and fluorescent spectra (right arrow) of PDNPs containing exciting spectrum and emission spectrum. Inset (D) is the image of PDNPs under visible (left) and UV (right) light. (For interpretation of the references to color in this figure legend, the reader is referred to the Web version of this article.)

catechol peak at 280 nm (Fig. 1D); this finding indicated the containing of a low proportion of 5,6-dihydroxyindole and dopamine units in PDNPs [52]. As for the fluorescence spectra, PDNPs had an optimal emission peak centered at 435 nm (excitation at 340 nm) with blue fluorescence under a UV lamp (Fig. 1D). The relative photoluminescence quantum yield was 2.2% with quinine sulfate in 0.1 M H_2SO_4 as a reference (Fig. S1). Furthermore, PDNPs illustrated a wavelength-dependent emission property (Fig. S2), suggesting a series of species originating from the self-assembly of oligomer and the units of dopamine and 5,6-dihydroxyindole in PDNPs [51]. Such different species will induce several different energy gaps and lead to variation of emission behavior [51].

The stability of PDNPs toward several ambient environments was evaluated in detail. Fig. S3A showed that the fluorescence intensity of PDNPs was constant at 435 nm against varying concentrations of NaCl from 0 mM to 100 mM, suggesting the excellent stability of PDNPs under high ionic conditions. Moreover, PDNPs had strong and relatively stable fluorescent activities in buffer with varying pH from 3 to 10 (Fig. S3B). The fluorescence intensity of PDNPs remained at ~90% after exposure to continuous light illumination at 340 nm for 60 min, indicating the high resistance to photobleaching (Fig. S3C). The excellent anti-photobleaching promoted the stability of PDNPs in common environments as proven by the fluorescence intensity maintained with a robust storage of more than 50 days (Fig. S3D).

The biocompatibility of the prepared PDNPs was assessed, as shown in Fig. S4. After incubation for 24 h with a series of concentrations of PDNPs, the cellular viability of A549 cells was high. The viability of A549 cells was 92% even when 500 μg/mL PDNPs were added. Thus, PDNPs have low cytotoxicity and good biocompatibility, suggesting their potential application potential in biomedicine containing biosensing.

3.2. Assessment and mechanism of the detection strategy for TRY activity based on PDNPs-Pro

The interaction system of Pro on PDNPs was investigated, as shown in Fig. 2 and Fig. S5. The fluorescence of PDNPs-Pro decreased significantly compared with that of pure PDNPs. The effective quenching may be due to the strong interaction between Pro and PDNPs in PDNPs-Pro. The quenched fluorescence of PDNPs caused by Pro in PDNPs-Pro was recovered with the addition of TRY. However, TRY at the level of 0.1 μg/mL had no effect on the fluorescence of PDNPs. These results indicated the feasibility to establish a simple fluorescence-activated detection method for TRY based on PDNPs-Pro.

Pro is rich arginine, which is the restriction site of TRY. Thus, the recovered fluorescence of PDNPs suggests the enzymatic hydrolysis of Pro by TRY [16], thereby causing PDNPs-Pro damage in this detection procedure. Therefore, the key role of this method is the fabrication of PDNPs-Pro with quenched PDNPs. At first, the possible change in PDNPs-Pro dispersion was investigated. As shown in Fig. 3A, with the introduction of the relatively low content of Pro, the original well-dispersed PDNPs aggregated with sizes ranging from 50 nm to hundreds of nanometers. PDNPs further assembled to large clusters when Pro concentration continuously increased (Fig. 3B), suggesting the phenomenon of aggregation caused PDNPs quenching in PDNPs-Pro [55]. In addition, photoluminescence lifetime and Stern-Volmer plot were carried out to evaluate the quenching mechanism of Pro to PDNPs in the fabricated PDNPs-Pro. As shown in Fig. S6, the average lifetime of PDNPs increased from 5.585 ns to 6.082 ns when Pro was added, indicating the increase in transition time from the excited state to the ground state of PDNPs aggregation caused by Pro in PDNPs-Pro [44]. Furthermore, the relative fluorescence intensities (F_0'/F', F_0' and F' were the fluorescence intensities of PDNPs in the absence and presence of variable Pro, respectively, as shown in supplementary material for detail.) and the Pro concentrations were expressed by Stern-Volmer plot with a perfect linear behavior ($R^2 = 0.998$), as shown in Fig. S7. According to equation S1 (shown in supplementary material), the bimodular quenching constant (Kq) was calculated to be 2.86×10^{14} M^{-1} s^{-1} [56]. Thus, the results of the aggregation behavior, changed lifetime and the larger Kq prove that PDNPs quenched by Pro is assigned to the static quenching (>kq~10^{10} M^{-1} s^{-1}) in the PDNPs-Pro, suggesting the formed non-fluorescent complexes between PDNPs and Pro [57].

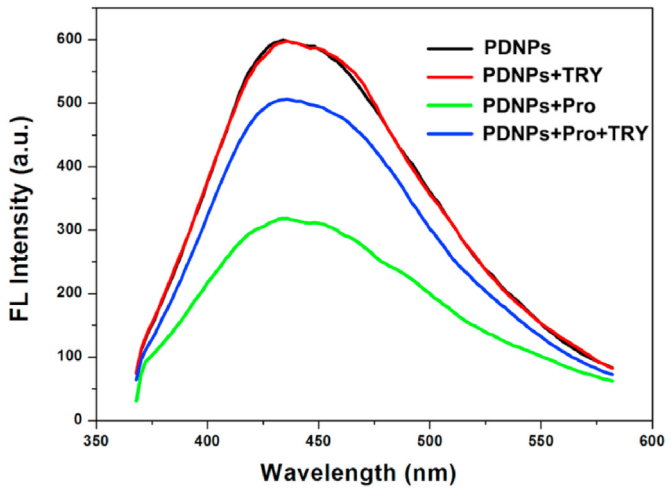

Fig. 2. Fluorescence spectra of PDNPs (0.15 μg/mL), PDNPs + TRY (0.1 μg/mL), PDNPs-Pro (40 μg/mL), and PDNPs-Pro with TRY in PB (pH 8.0) with the excitation at 340 nm.

In general, cationic proteins can interact with anionic organic or inorganic precursors through appropriate modes to promote the condensation, assembly, or hydrolysis of anionic units [58–60]. Therefore, the driving forces of PDNPs-Pro formation were evaluated. The zeta potential of the reaction system of PDNPs-Pro was determined. As shown in Fig. 3C, the zeta potentials of Pro and PDNPs were 2.1 mV and −3.9 mV, respectively, whereas the zeta potential of PDNPs-Pro was −0.8 mV. While, the positive Pro was ascribed to that interacting pH value (8.0) was less than the isoelectric point (pI) of Pro (pI = 12.0). As such, the presence of electrostatic interaction in the binding system of PDNPs-Pro was revealed. The polydopamine layer or nanoparticles were generally negatively charged due to the outward −OH [53], thereby inducing an electrostatic interaction between negatively charged PDNPs and positive Pro. In addition, PDNPs-Pro kept the relatively constant fluorescence at variable solution with changed pH (Fig. S8), suggesting the stable formed aggregation of PDNPs and Pro. However, unlike the interaction of protein and graphene quantum dots [16], reports on the assembly of fluorescent nanostructured polydopamine and positive protein through electrostatic interaction were rare. Other effective factors may participate in the control of such abovementioned mixture. FTIR was employed to investigate the variable functional groups in PDNPs-Pro. As shown in Fig. 3D, the band at 3441 cm^{-1} related to the stretching vibration of O–H and N–H of PDNPs shifts to 3413 cm^{-1} for PDNP-Pro. The bands assigned to the stretching vibration of O–H and N–H of Pro, which were at 3438 and 1650 cm^{-1}, respectively, shifted to 3413 and 1638 cm^{-1} for the PDNP-Pro. These absorption peaks that shifted to a lower wavelength number could be explicated through the strong hydrogen bond between −NH and −OH from PDNPs and Pro in PDNPs-Pro [61]. In general, the adsorption or assembly between protein and nanomaterials is related to the electric charge, the ability of the protein to form hydrogen bond, and the size, shape, and surface modification of nanomaterials in a certain solution condition [62,63].

Aside from the electrostatic interaction and hydrogen bond, the effect of the particle size on possible quenching by Pro was also investigated. Another kind of fluorescent polydopamine nanoparticles with different diameter (named as PD2 in this work) was fabricated following a reported method [64] (See supplementary materials for details.). The obtained PD2 exhibited the emission spectrum centered at 440 nm of 350 nm excitation, and a bright blue image of PD2 was obtained under the irradiating with a 365 nm lamp (Fig. S9), suggesting the excellent fluorescence property. The TEM image (Fig. S10A) showed quasi-sphere morphology with an average diameter of 18 nm, which was similar to those in the previous report [64]. However, PD2 was different from PDNPs because it cannot be quenched by Pro even at high concentrations (Figs. S10B and C). Moreover, a good dispersion of PD2 with an interval combined with distributed Pro in the mixture of PD2 and Pro was found by TEM (white circle in Fig. S10D); thus, the size of the fluorescent nanostructured polydopamine was also a major factor that affected the integration with Pro. The different quenching behavior between PDNPs and PD2 caused by Pro reveal the following reasons that cause the integration of PDNPs and Pro. The average axial distance between two adjacent amino acids is approximately 0.35 nm, and the linear size of Pro reaches 14 nm based on the average number of amoid acids of Pro is approximately 40. This size enables the positively charged Pro to absorb the small-scale and negative PDNPs through electrostatic interaction and hydrogen bonds; thus, several PDNPs aggregate for the assembly between Pro and PDNPs in PDNPs-Pro. Then, quenching occurs as a result of aggregation [27,28,65]. Thus, appropriate size combined with the surface charge and hydrogen bonds are the key factors for fabricating the aggregation-caused

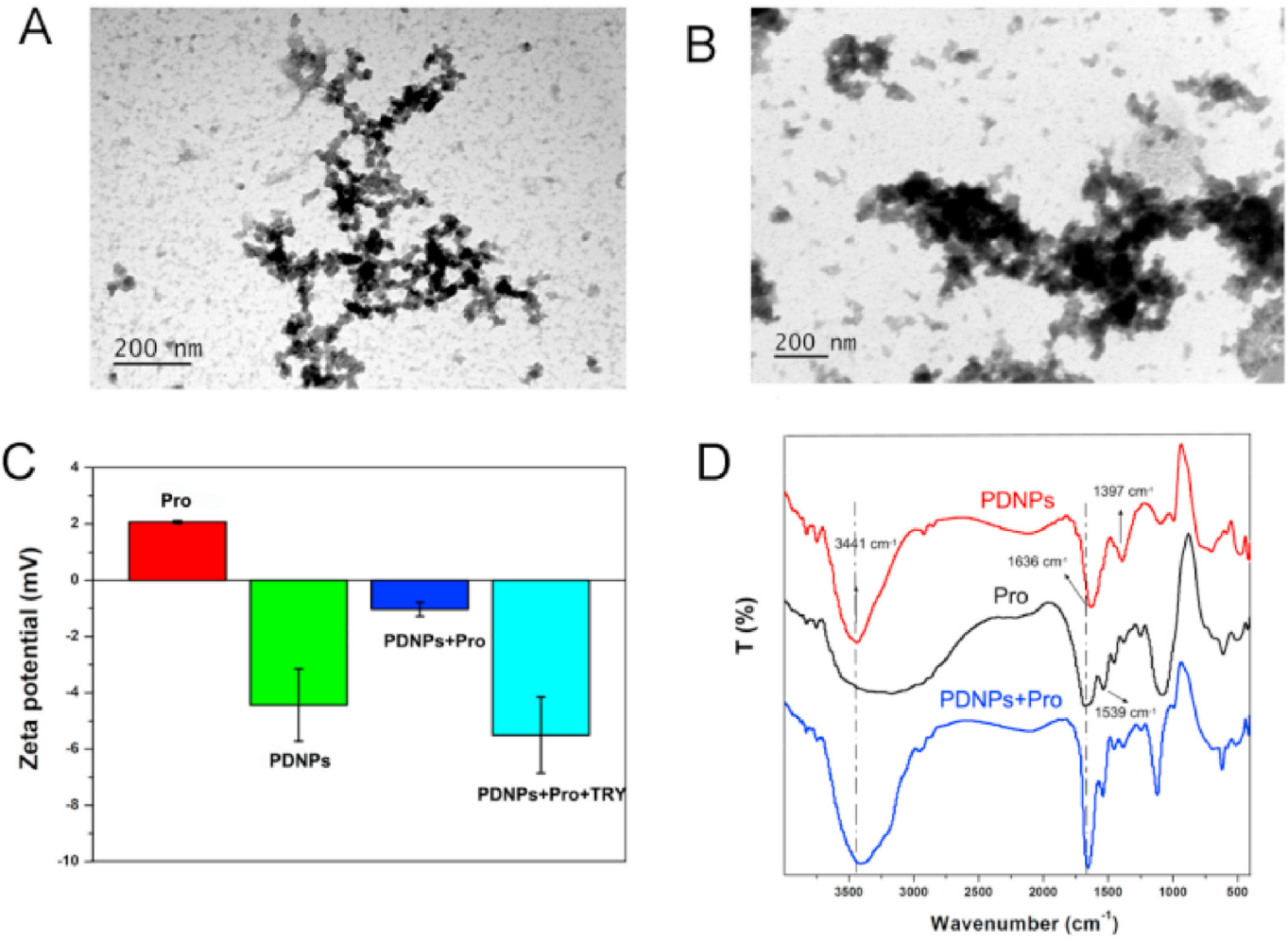

Fig. 3. TEM images of PDNPs in the presence of (A) 30 μg/mL of Pro; (B) 40 μg/mL of Pro. (C) Zeta potential histogram of Pro, PDNPs, PDNPs-Pro, and PDNPs-Pro with TRY. (D) FTIR spectra of PDNPs, Pro, and PDNPs-Pro.

quenching system on the basis of the fluorescent nanostructured polydopamine and the protein. While, it is necessary to point out that the quenching mechanism illustrated herein is based on the different phenomenon of Pro to PDNPs and PD2. The detailed mechanism about the controlled-size of fluorescent nanostructured polydopamine and Pro or other proteins needs further verification.

The wreck of PDNPs-Pro caused by TRY for TRY monitoring was further monitored using UV–vis and dynamic light scattering (DLS). As shown in Fig. 4A, the absorption intensity of PDNPs-Pro at 300–800 nm increased, and TRY addition obviously reduced the absorption at 300–800 nm compared with the PDNPs absorption spectrum. The reacted solution of PDNPs-Pro with TRY exhibited an absorption spectrum similar to that of pure PDNPs. The recovered changes of the UV–vis absorption spectra (Fig. 4A) revealed the good release and wide dispersion of PDNPs from PDNPs-Pro. As shown in Fig. 4B, DLS confirmed the small size of the PDNPs with a hydrodynamic diameter of around 5 nm, which was in accordance with the TEM result (Fig. 1A). However, the PDNPs-Pro in aqueous solution had a wide size distribution centered at ~460 nm. When TRY was added, the particle size of the system decreased to 84 nm with a narrow distribution range, indicating the cleavage of the arginine-rich Pro induced by TRY. The results confirm the assembly of PDNPs and Pro and the disassembly induced by TRY, suggesting the effective sensing potential for TRY based on the developed PDNPs-Pro.

3.3. Optimization of experimental conditions

Several experimental conditions were optimized to determine the best performance of the fluorescence assay. The quenching degree of PDNPs by variable content Pro was investigated. With the increase of Pro concentration from 10 to 60 μg/mL, PDNPs were gradually quenched and almost entirely quenched when 40 μg/mL of Pro was added (Fig. S11A). Thus, 40 μg/mL of protamine was selected as the optimal quenching content for the assay of TRY based on PDNPs-Pro. The quenching dynamics of Pro to PDNPs was monitored at a different time to obtain the suitable quenching condition. PDNPs were quickly quenched by Pro in short time, and then the thoroughly quenched status was reached and maintained at a steady stage in a 20 min period (Fig. S11B). PDNPs that reacted with Pro for 2 min were chosen for TRY detection to ensure complete quenching.

The investigation of the optimal enzymatic conditions of pH of the medium, hydrolyzed temperature and incubated time for TRY was carried out. First, the effects of pH on fluorescence enhancement efficiency $(F-F_0)/F_0$ were investigated in the range of 6.5–9 (Fig. S12A). Thus, pH 8.0 is the appropriate pH condition for TRY. Then, the TRY hydrolyzed processes at different temperatures were examined (Fig. S12B). $(F-F_0)/F_0$ at 37 °C was higher than other

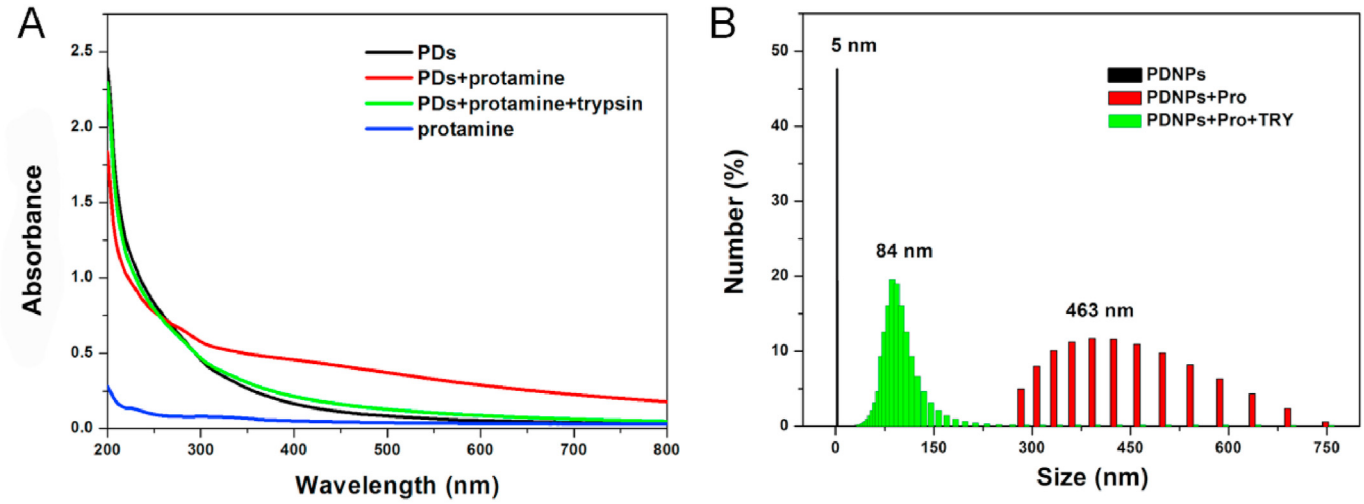

Fig. 4. (A) UV−vis absorption spectra of PDNPs, PDNPs-Pro, PDNPs-Pro with TRY, and Pro. (B) DLS of PDNPs, PDNPs-Pro, and PDNPs-Pro with TRY.

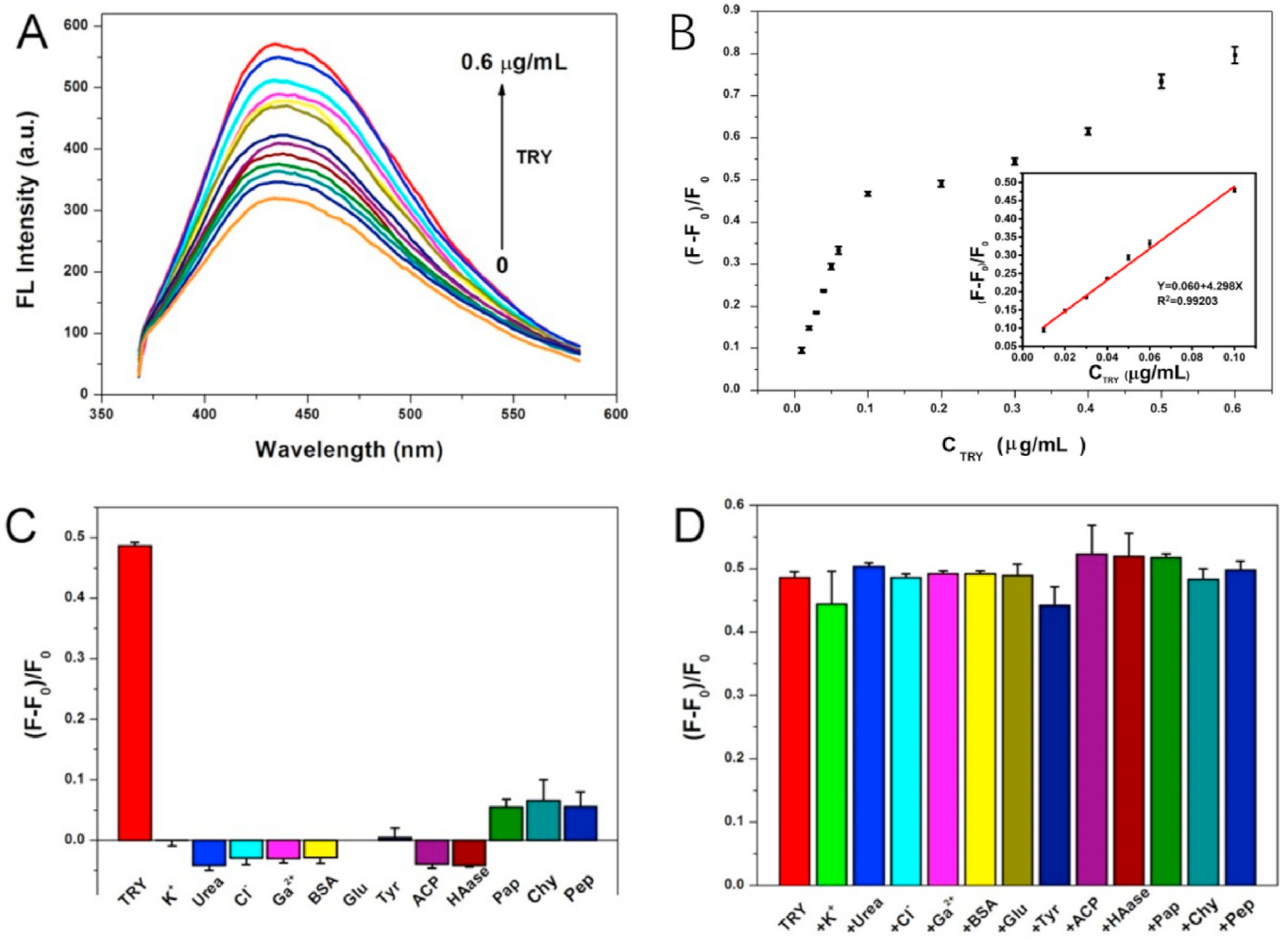

Fig. 5. (A) Fluorescence emission spectra of the PDNPs-Pro mixture upon the addition of various concentrations of TRY. (B) Plots of fluorescence enhancement efficiency with increasing of C_{TRY}. Inset: the linear fitting plot with various TRY. (C) Fluorescent enhancement efficiency of PDNPs-Pro upon the addition of TRY (0.1 μg/mL) or one of the interferences. (D) Fluorescent enhancement efficiency of PDNPs-Pro with TRY (0.1 μg/mL) in the absence or the presence of one interference. (10 μg/mL of K^+, Cl^-, Ca^{2+}, glucose, urea, BSA and papain; and 1.2 U/mL of tyrosinase, ACP, hyaluronidase pepsin, and Chy). Error bars are the SDs of three independent experiments. All experiments were conducted in 10 mM PB (pH 8.0).

operating temperature, suggesting that the testing condition at 37 °C was ideal with the consideration of physiological temperature. Furthermore, with increasing reaction time, $(F-F_0)/F_0$ at three temperatures increased rapidly in the first 20 min, thereby reaching the plateau after 45 min. Therefore, the ideal reacting conditions for TRY work were 37 °C and 45 min at pH 8.0.

3.4. TRY activity detection

Under the optimal conditions, the variable fluorescence intensity of PDNPs-Pro controlled by the addition of variable TRY was investigated. Fig. 5A showed that the fluorescence intensity centered at 435 nm was gradually restored along with the increased TRY. Then, the fluorescence signal was almost completely recovered when the TRY concentration reached 0.6 μg/mL. Fig. 5B showed the plots of $(F-F_0)/F_0$ against TRY concentration. Moreover, with the concentration of TRY in the range of 0.01–0.1 μg/mL, fluorescence enhancement efficiency exhibited the linear fitting equation of $(F-F_0)/F_0 = 0.060 + 4.298C_{TRY(\mu g/mL)}$ ($R^2 = 0.992$). The limit of detection was 6.7 ng/mL based on the calculation from S/N = 3. Compared with other reported optical methods for TRY, this PDNPs-based probe displayed a comparable performance with other optical analytical methods for TRY determination (Table S1). Furthermore, this strategy exhibits the advantages of free surface modification, homogeneous and convenient mixing procedure, cost effectiveness, and the green preparation of PDNPs with long stability and high biosafety.

The effects of other proteases and ions on the response of PDNPs-Pro were compared to evaluate the selectivity of this strategy for TRY. As shown in Fig. 5C, PDNPs-Pro reacted with various potential substances, such as ions, proteins, enzymes and other proteases. The results clearly showed that, except for TRY, interferences had negligible effectiveness on the testing system of PDNPs-Pro. Furthermore, the results of the fluorescence responses of the coexisting interference and TRY on PDNPs-Pro(Fig. 5D) exhibited almost the same degree with that of simple TRY on PDNPs-Pro, even in the coexistence of other protease. Moreover, SDS-PAGE electrophoresis of Pro interacting with TRY and different proteases was respectively performed to evaluate the possible change of Pro, as shown in Fig. S13. It showed that only TRY obviously digested Pro and induced small protein band. While, other proteases had little effect on Pro under the reacting condition, confirming the feasibility of this method for TRY testing excluding the disturbing from other proteases. Thus, the developed method for TRY monitoring exhibited excellent selectivity and reliability.

Spiking tests were carried out by adding four levels of TRY into the 10% human serum samples to further evaluate the potential application of the proposed method for TRY assay in clinical diagnosis. As shown in Table S2, the recovery of TRY at different concentrations in serum was in the range of 98.0%–109.8% with relative standard deviations less than 3%, indicating that the method based on PDNPs developed here can be applied for the accurate detection of TRY in real samples.

3.5. Inhibitor screening

TRY inhibitors can not only be applied as drugs to treat related diseases but also play significant roles in drug development. Thus, developing a new convenient method for protease inhibitor screening is important. The inhibitor from soybean, which could restrain the cleavage of arginine sites by inactivating TRY, was applied to validate the practicability of the prepared PDNPs-Pro. As shown in Fig. S14, the inhibition efficiency increased gradually with the addition of the inhibitor. IC50, which represents the required concentration of the inhibitor that suppresses 50% enzymatic activity of TRY, was 0.25 μg/mL, which is comparable to reported results [9,66]. The results suggest that this simple method can be applied for protease activity detection and the inhibitor screening well.

4. Conclusion

Positively charged blue-light PDNPs with appropriate surface group and size are effectively prepared via the hydroxyl radical-induced degradation of PDA nanoparticles. The obtained PDNPs exhibit stable fluorescence property and high biocompatibility. To the best of our knowledge, PDNPs with appropriate size, are developed for the first time as assembly unit with protein (like Pro in this work) to generate integration via the electrostatic interaction and hydrogen bond. As such, PDNPs-Pro with aggregation-induced quenching was fabricated. A fluorescence assay is developed for the simple, sensitive, and selective determination of TRY activity on the basis of PDNPs-Pro hydrolysis by TRY and the release of PDNPs. Apart from the satisfactory analytical performance of this TRY detection method, it has the obvious advantages of unnecessary complicated surface modification, easy material preparation, simple testing procedure, and low cost than other reported TRY detection strategies. In addition, this method has excellent practicability in human serum samples and feasibility of TRY inhibitor screening. Furthermore, this work may provide an idea for the control of PDNPs surface property and particle size on the interaction between PDNPs and biological target molecules for widespread applications.

CRediT authorship contribution statement

Fenglan Li: Methodology, Data curation, Formal analysis, Visualization, Funding acquisition, Writing - original draft, Writing - review & editing. **Yiping Chen:** Data curation, Formal analysis, Writing - review & editing. **Renxi Lin:** Data curation, Formal analysis. **Chenfang Miao:** Data curation, Formal analysis. **Jiahui Ye:** Data curation, Formal analysis. **Qianqian Cai:** Data curation, Formal analysis. **Zhengjun Huang:** Resources. **Yanjie Zheng:** Resources. **Xinhua Lin:** Resources. **Zongfu Zheng:** Project administration, Funding acquisition. **Shaohuang Weng:** Conceptualization, Formal analysis, Project administration, Supervision, Funding acquisition, Writing - original draft, Writing - review & editing.

Declaration of competing interest

The authors declare no competing interest.

Acknowledgment

The authors gratefully acknowledge for financial support from the National Natural Science Foundation of China (21405016, 21775023, 21705021), Joint Funds for the innovation of science and Technology, Fujian province (2017Y9121, 2017Y9124),the National Science Foundation of Fujian Province (2020J01626). Fenglan Li thanks the Start Fund for Scientific Research, Fujian Medical University (2018QH2018).

Appendix A. Supplementary data

Supplementary data to this article can be found online at https://doi.org/10.1016/j.aca.2021.338201.

References

[1] L. Zhang, J. Du, A sensitive and label-free trypsin colorimetric sensor with

cytochrome c as a substrate, Biosens. Bioelectron. 79 (2016) 347–352.
[2] J.C. Powers, J.L. Asgian, O.D. Ekici, K.E. James, Irreversible inhibitors of serine, cysteine, and threonine proteases, Chem. Rev. 102 (2015) 4639–4750.
[3] M. Hirota, M. Ohmuraya, H.J. Baba, The role of trypsin, trypsin inhibitor, and trypsin receptor in the onset and aggravation of pancreatitis, Gastroenterol. 41 (2006) 832–836.
[4] J.M. Artigas, M.E. Garcia, M.R. Faure, A.M. Gimeno, Serum trypsin levels in acute pancreatic and non-pancreatic abdominal conditions, Postgrad. Med. 57 (1981) 219–222.
[5] X.Y. Lin, Z.M. Zhu, C.F. Zhao, S.G. Li, Q.C. Liu, A.L. Liu, L.Q. Lin, X.H. Lin, Robust oxidase mimicking activity of protamine-stabilized platinum nanoparticles units and applied for colorimetric sensor of TRY and inhibitor, Sens. Actuators, B 284 (2019) 346–353.
[6] M.A. Seia, P.W. Stege, S.V. Pereira, E.E. De Vito, J. Raba, G.A. Messina, Silica nanoparticle-based microfluidic immunosensor with laser-induced fluorescence detection for the quantification of immunoreactive trypsin, Anal. Biochem. 463 (2014) 31–37.
[7] X. You, Y. Li, B. Li, J. Ma, Gold nanoclusters-based chemiluminescence resonance energy transfer method for sensitive and label-free detection of trypsin, Talanta 147 (2016) 63–68.
[8] S.H. Weng, Q.C. Liu, C.F. Zhao, G.L. Hong, Z.Q. Jiang, L.Q. Lin, Y.Z. Chen, X.H. Lin, Sensitive electrochemical immunoassay based on polythionine-Au nanocomposites as enhanced sensing signal for selective detection of biomarker with high isoelectric point, Sens. Actuators, B 216 (2015) 307–315.
[9] H. Dai, S. Chen, Y. Li, B. Zeng, S. Zhang, Z. Hong, Y.Y. Lin, Photoelectrochemical biosensor constructed using TiO_2 mesocrystals based multipurpose matrix for trypsin detection, Biosens. Bioelectron. 92 (2017) 687–694.
[10] L. Zhao, T. Wang, Q. Wu, Y. Liu, Z. Chen, X. Li, Fluorescent strips of electrospun fibers for ratiometric sensing of serum heparin and urine trypsin, ACS Appl. Mater. Interfaces 9 (2017) 3400–3410.
[11] M.H. Chen, Q. Wen, F.L. Gu, J.W. Gao, C.C. Zhang, Q.M. Wang, Mussel chemistry assembly of a novel biosensing nanoplatform based on polydopamine fluorescent dot and its photophysical features, Chem. Eng. J. 342 (2018) 331–338.
[12] L.H. Bai, H.X. Yan, Y.B. Feng, W.X. Feng, L.Y. Yuan, Multi-excitation and single color emission carbon dots doped with silicon and nitrogen: synthesis, emission mechanism, Fe^{3+} probe and cell imaging, Chem. Eng. J. 373 (2019) 963–972.
[13] M. Wang, D. Su, G. Wang, X.G. Su, A fluorometric sensing method for sensitive detection of TRY and its inhibitor based on gold nanoclusters and gold nanoparticles, Anal. Bioanal. Chem. 410 (2018) 6891–6900.
[14] M. Liu, J. Zhou, Y. He, Z. Cai, Y. Ge, J. Zhou, G. Song, ε-Poly-L-lysine-protected Ti_3C_2MXene quantum dots with high quantum yield for fluorometric determination of cytochrome c and trypsin, Microchim. Acta 186 (2019) 770.
[15] D. Kim, J. Kim, T.S. Lee, Dual-signal detection of trypsin using controlled aggregation of conjugated polymer dots and magnetic nanoparticles, Sens. Actuators, B 264 (2018) 45–51.
[16] Y. Lin, R. Chapman, M.M. Stevens, Label-free multimodal protease detection based on protein/perylene dye coassembly and enzyme-triggered disassembly, Anal. Chem. 86 (2014) 6410–6417.
[17] G.L. Wang, F. Yuan, T.T. Gu, Y.M. Dong, Q. Wang, W.W. Zhao, Enzyme-initiated quinone-chitosan conjugation chemistry: toward a general in situ strategy for high-throughput photoelectrochemical enzymatic bioanalysis, Anal. Chem. 90 (2018) 1492–1497.
[18] F.M. Zhang, L.B. Xu, Q.N. Zhao, Y. Sun, X.H. Wang, P.Y. Ma, D.Q. Song, Dopamine-modified Mn-doped ZnS quantum dots fluorescence probe for the sensitive detection of tyrosinase in serum samples and living cells imaging, Sens. Actuators, B 256 (2018) 1069–1077.
[19] S. Krishnamurthy, P.V. Kamat, CdSe-graphene oxide light-harvesting assembly: size-dependent electron transfer and light energy conversion aspects, ChemPhysChem 15 (2014) 2129–2135.
[20] B. Andreiuk, A. Reisch, E. Bernhardt, A.S. Klymchenko, Fighting aggregation-caused quenching and leakage of dyes in fluorescent polymer nanoparticles: universal role of counter ion, Chem. Asian J. 14 (2019) 836–846.
[21] Y. Guo, Y. Hu, Z. Deng, DNA Directed self-assembly of fluorescent colloidal semiconductor quantum dots and plasmonic metal nanoparticles heterogeneous nanomaterials, Chin. J. Chem. 34 (2016) 259–264.
[22] X. Ji, N.S. Makarov, W.T. Wang, G. Palui, I. Robel, H.J. Mattoussi, Tuning the redox coupling between quantum dots and dopamine in hybrid nanoscale assemblies, J. Phys. Chem. C 119 (2015) 3388–3399.
[23] F. Aldeek, X. Ji, H. Mattoussi, Quenching of quantum dot emission by fluorescent gold clusters: what it does and does not share with the forster formalism, J. Phys. Chem. C 117 (2013) 15429–15437.
[24] J. Hu, X. Bai, Y. Liu, X. Liao, Functionalized carbon quantum dots with dopamine for tyrosinase activity analysis, Anal. Chim. Acta 995 (2017) 99–105.
[25] H. Ao, Z. Qian, Y. Zhu, M. Zhao, C. Tang, Y. Huang, H. Feng, A. Wang, A fluorometric biosensor based on functional Au/Ag nanoclusters for real-time monitoring of tyrosinase activity, Biosens. Bioelectron. 86 (2016) 542–547.
[26] Z. Qian, L. Chai, Q. Zhou, Y. Huang, C. Tang, J. Chen, H. Feng, Reversible fluorescent nanoswitch based on carbon quantum dots nanoassembly for real-time acid phosphatase activity monitoring, Anal. Chem. 87 (2015) 7332–7339.
[27] V. Ramanan, B. Siddaiah, K. Raji, P. Ramamurthy, Green synthesis of multifunctionalized, nitrogen-doped, highly fluorescent carbon dots from waste expanded polystyrene and its application in the fluorimetric detection of Au^{3+}ions in aqueous media, ACS Sustain. Chem. Eng. 6 (2018) 1627–1638.
[28] D. Hühn, K. Kantner, C. Geidel, S. Brandholt, I. De Cock, S.J. Soenen, P. Rivera Gil, J.M. Montenegro, K. Braeckmans, K. Müllen, G.U. Nienhaus, M. Klapper, W.J. Parak, Polymer-coated nanoparticles interacting with proteins and cells: focusing on the sign of the net charge, ACS Nano 7 (2013) 3253–3263.
[29] Y. Lin, R. Chapman, M.M. Stevens, Integrative self-assembly of graphene quantum dots and biopolymers into a versatile biosensing toolkit, Adv. Funct. Mater. 25 (2015) 3183–3192.
[30] Q. Miao, C. Xie, X. Zhen, Y. Lyu, H. Duan, X. Liu, J. Jokerst, K.Y. Pu, Molecular afterglow imaging with bright, biodegradable polymer nanoparticles, Nat. Biotechnol. 35 (2017) 1102–1110.
[31] K.Y. Pu, A.J. Shuhendler, J.V. Jokerst, J. Mei, S.S. Gambhir, Z.N. Bao, J. Rao, Semiconducting polymer nanoparticles as photoacoustic molecular imaging probes in living mice, Nat. Biotechnol. 9 (2014) 233–239.
[32] A. Reisch, A.S. Klymchenko, Fluorescent polymer nanoparticles based on dyes: seeking brighter tools for bioimaging, Small 12 (2016) 1968–1992.
[33] X. Wang, L. Liu, S. Zhu, L. Li, Fluorescent platforms based on organic molecules for chemical and biological detection, Phys. Status Solidi-R. 13 (2019), 1800521.
[34] Y.Y. Liu, K.L. Ai, L.H. Lu, Polydopamine and its derivative materials: synthesis and promising applications in energy, environmental, and biomedical fields, Chem. Rev. 114 (2014) 5057–5115.
[35] J.H. Ryu, P.B. Messersmith, H. Lee, Polydopamine surface chemistry: a decade of discovery, ACS Appl. Mater. Interfaces 10 (2018) 7523–7540.
[36] W. Cheng, X. Zeng, H. Chen, Z. Li, W. Zeng, L. Mei, Y. Zhao, Versatile polydopamine platforms: synthesis and promising applications for surface modification and advanced nanomedicine, ACS Nano 13 (2019) 8537–8565.
[37] S.E. Yakhlifi, V. Ball, Polydopamine as a stable and functional nanomaterial, Colloids Surf.: Biointerfaces 186 (2020), 110719.
[38] S.H. Xu, Y.Y. Nie, L.P. Jiang, J. Wang, G.Y. Xu, W. Wang, X.L. Luo, Polydopamine nanosphere/gold nanocluster (Au NC)-based nanoplatform for dual color simultaneous detection of multiple tumor-related microRNAs with DNase-I-assisted target recycling amplification, Anal. Chem. 90 (2018) 4039–4045.
[39] Y. Xie, X. Lin, Y. Huang, R. Pan, Z. Zhu, L.J. Zhou, C.Y. Yang, Highly sensitive and selective detection of miRNA: DNase I-assisted target recycling using DNA probes protected by polydopamine nanospheres, Chem. Commun. 51 (2015) 2156–2158.
[40] Y. Jiang, Y. Tang, P. Miao, Polydopamine nanosphere@silver nanoclusters for fluorescence detection of multiplex tumor markers, Nanoscale 11 (2019) 8119–8123.
[41] B. Liu, X. Han, J.W. Liu, Iron oxide nanozyme catalyzed synthesis of fluorescent polydopamine for light-up Zn^{2+} detection, Nanoscale 8 (2016) 13620–13626.
[42] X.J. Kong, S. Wu, T.T. Chen, R.Q. Yu, X. Chu, MnO_2-induced synthesis of fluorescent polydopamine nanoparticles for reduced glutathione sensing in human whole blood, Nanoscale 8 (2016) 15604–15610.
[43] H. Yin, K. Zhang, L. Wang, K. Zhou, J. Zeng, D. Gao, Z. Xia, Q. Fu, Redox modulation of polydopamine surface chemistry: a facile strategy to enhance the intrinsic fluorescence of polydopamine nanoparticles for sensitive and selective detection of Fe^{3+}, Nanoscale 10 (2018) 18064–18073.
[44] Q. Ci, J. Liu, X. Qin, L. Han, H. Li, H. Yu, K. Lim, C. Zhang, N. Li, W. Huang, Polydopamine dots-based fluorescent nanoswitch assay for reversible recognition of glutamic acid and Al^{3+} in human serum and living cell, ACS Appl. Mater. Interfaces 10 (2018) 35760–35769.
[45] T. Xiao, J. Sun, J. Zhao, S. Wang, G. Liu, X. Yang, FRET effect between fluorescent polydopamine nanoparticles and MnO_2 nanosheets and its application for sensitive sensing of alkaline phosphatase, ACS Appl. Mater. Interfaces 10 (2018) 6560–6569.
[46] Y.Y. Zhao, L. Li, R.Q. Yu, T.T. Chen, X. Chu, CoOOH-induced synthesis of fluorescent polydopamine nanoparticles for the detection of ascorbic acid, Anal. Methods 9 (2017) 5518–5524.
[47] Y. Liu, W. Shen, H. Cui, Metal ion-induced chemiluminescence recovery for highly intensive chemiluminescence bifunctionalized polydopamine nanospheres, J. Mater. Chem. C 7 (2019) 14588–14593.
[48] R.B. Guo, B. Chen, F.L. Li, S.H. Weng, Z.F. Zheng, M. Chen, W. Wu, X.H. Lin, C.Y. Yang, Positive carbon dots with dual roles of nanoquencher and reference signal for the ratiometric fluorescence sensing of DNA, Sens. Actuators, B 264 (2018) 193–201.
[49] J.Y. Huang, F.L. Li, R.B. Guo, Y.Y. Chen, Z.Z. Wang, C.F. Zhao, Y.J. Zheng, S.H. Weng, X.H. Lin, A signal-on ratiometric fluorometric heparin assay based on the direct interaction between amino-modified carbon dots and DNA, Microchim. Acta 185 (2018) 260.
[50] F.L. Li, Q.Q. Cai, X.L. Hao, C.F. Zhao, Z.J. Huang, Y.J. Zheng, X.H. Lin, S.H. Weng, Insight into the DNA adsorption on nitrogen-doped positive carbon dots, RSC Adv. 9 (2019) 12462–12469.
[51] J.H. Lin, C.J. Yu, Y.C. Yang, W.L. Tseng, Formation of fluorescent polydopamine dots from hydroxyl radical-induced degradation of polydopamine nanoparticles, Phys. Chem. Chem. Phys. 17 (2015) 15124–15130.
[52] Y.Y. Chen, Z.Z. Wang, X.L. Hao, F.L. Li, Y.J. Zheng, J.Z. Zhang, X.H. Lin, S.H. Weng, Selective and sensitive fluorescent monitoring of acid phosphatase (ACP) activity under neutral conditions through the ACP enzymatic catalysis of dopamine as a new substrate to polydopamine, Sens. Actuators, B 297 (2019) 126784.
[53] S.H. Weng, D. Liang, H.Z. Qiu, Z.E. Liu, Z. Lin, Z.F. Zheng, A.L. Liu, W. Chen, X.H. Lin, A unique turn-off fluorescent strategy for sensing dopamine based on formed polydopamine (pDA) using graphene quantum dots (GQDs) as fluorescent probe, Sens. Actuators, B 221 (2015) 7–14.

[54] N.F. Della Vecchia, R. Avolio, M. Alfè, M.E. Errico, A. Napolitano, M. d'Ischia, Building-block diversity in polydopamine underpins a multifunctional eumelanin-type platform tunable through a quinone control point, Adv. Funct. Mater. 23 (2013) 1331–1340.
[55] M. Nurunnabi, Z. Khatun, M. Nafiujjaman, D.G. Lee, Y.K. Lee, Surface coating of graphene quantum dots using mussel-inspired polydopamine for biomedical optical imaging, ACS Appl. Mater. Interfaces 5 (2013) 8246–8253.
[56] Y. Ma, A. Chen, Y. Huang, X. He, X. Xie, B. He, J. Yang, X. Wang, Off-on fluorescent switching of boron-doped carbon quantum dots for ultrasensitive sensing of catechol and glutathione, Carbon 162 (2020) 234–244.
[57] X. Sun, Y. Wang, Y. Lei, Fluorescence based explosive detection: from mechanisms to sensory materials, Chem. Soc. Rev. 44 (2015) 8019–8061.
[58] Y. Jiang, D. Yang, L. Zhang, L. Li, Q. Sun, Y. Zhang, J. Li, Z. Jiang, Biomimetic synthesis of titania nanoparticles induced by protamine, Dalton Trans. 31 (2008) 4165–4171.
[59] S.L. Sewell, D.W. Wright, Biomimetic synthesis of titanium dioxide utilizing the R5 peptide derived from cylindrotheca fusiformis, Chem. Mater. 18 (2006) 3108–3113.
[60] F. Kurayama, S. Suzuki, T. Oyamada, T. Furusawa, M. Sato, N. Suzuki, Facile method for preparing organic/inorganic hybrid capsules using amino-functional silane coupling agent in aqueous media, J. Colloid Interface Sci. 349 (2010) 70–76.
[61] S. Ahmadzadeh, S. Desobry, J. Keramat, A. Nasirpour, Crystalline structure and morphological properties of porous cellulose/clay composites: the effect of water and ethanol as coagulants, Carbohydr. Polym. 141 (2016) 211–219.
[62] J.F. Hou, Y.L. Yang, C. Wang, Molecular mechanisms of interface interactions between nanomaterials and proteins, Acta Phys. Chim. Sin. 33 (2017) 63–79.
[63] D.M. Basalyga, R.A.J. Latour Jr., Theoretical analysis of adsorption thermodynamics for charged peptide residues on SAM surfaces of varying functionality, Biomed. Mater. Res. A 1 (2003) 120–130.
[64] X. Zhang, S. Wang, L. Xu, L. Feng, Y. Ji, L. Tao, S. Li, Y. Wei, Biocompatible polydopamine fluorescent organic nanoparticles: facile preparation and cell imaging, Nanoscale 4 (2012) 5581–5584.
[65] M. Xie, F. Zhang, L. Liu, Y. Zhang, Y. Li, H. Li, J. Xie, Surface modification of graphene oxide nanosheets by protamine sulfate/sodium alginate for anticancer drug delivery application, Appl. Surf. Sci. 440 (2018) 853–860.
[66] Z.Z. Hu, Y.X. Li, E. Hussain, X.N. Huang, Y.Y. Zhang, N. Niu, S.A. Shahzad, C. Yu, Black phosphorus nanosheets based sensitive protease detection and inhibitor screening, Talanta 197 (2019) 270–276.